



Tikrit Journal of Pure Science

ISSN: 1813 – 1662 (Print) --- E-ISSN: 2415 – 1726 (Online)

Journal Homepage: <http://tjps.tu.edu.iq/index.php/j>



Synthesis, Characterization, and Biological Evaluation of New Hg(II) Complexes of (2-(2-(2-chlorobenzylidene)hydrazineyl)benzothiazole with Phosphine Ligands

Alaa H. Ali¹, Ahmed A. Irzoqi¹, Pramod K. Singh²

¹ Department of Chemistry, College of Education for Pure Science, University of Tikrit, Tikrit, Iraq

² COE in Solar Cells & Renewable Energy, Department of Physics, Sharda University, Greater Noida, India

ARTICLE INFO.

Article history:

-Received: 2 / 10 / 2023
 -Received in revised form: 3 / 11 / 2023
 -Accepted: 12 / 11 / 2023
 -Final Proofreading: 7 / 1 / 2024
 -Available online: 25 / 4 / 2024

Keywords: 2-Mercaptobenzothiazole, Hg Complexes, 2-chlorobenzaldehyde, Schiff base, Heterocycle Compound, Diphosphines, Antibacterial.

Corresponding Author:

Name: Ahmed A. Irzoqi

E-mail: ahmedirzoqi@tu.edu.iq

Tel:

©2024 THIS IS AN OPEN ACCESS ARTICLE UNDER THE CC BY LICENSE

<http://creativecommons.org/licenses/by/4.0/>



ABSTRACT

The Synthesis of new Hg(II) complexes of (2-(2-(2-chlorobenzylidene) hydrazineyl)benzothiazole) (CHB) with phosphine ligands (dppm, dppe, dppp, and dppb) were synthesized, resulting in complexes with the following formulas: $[\text{Hg}_2(\text{CHB})_2(\mu\text{-dppm})_2]\text{Cl}_4$ or $[\text{Hg}_2(\text{CHB})_2(\mu\text{-phosphine})\text{Cl}_2]\text{Cl}_2$ (where the phosphines are dppe, dppp and dppb). The suggested geometry around the metal ion is tetrahedral, with the (CHB) ligand acting as a bidentate ligand through the N atoms, while the phosphine ligands act as bidentate bridging ligands through the P atoms. The prepared complexes were characterized various analytical techniques including molar conductivity, infrared spectra, $^{31}\text{P}\{^1\text{H}\}$ -NMR, ^1H -NMR, and ^{13}C -NMR spectra. Additionally, the biological effectiveness of these complexes was evaluated against four types of bacteria, namely *Streptococcus faecalis*, *Staphylococcus aureus*, *Escherichia coli* and *Pseudomonas aeruginosa*, has been assessed. Some of the complexes exhibited an inhibition level in the range of (5-10 mm) at the minimum inhibitory concentration indicating potential antibacteria properties.

تحضير وتشخيص والتقييم الحيوي لمعقدات الزئبق (II) الجديدة من (2)-(2)-(2-كلوربنزيلدين)

هيدرازينيل) بنزوئثيازول مع ليكاندات الفوسفين

علاء حمد علي¹، أحمد عبدالستار إرزوقي¹، برامود كومار سينغه²

¹ قسم الكيمياء، كلية التربية للعلوم الصرفة، جامعة تكريت، تكريت، العراق

² المركز المتميز في الخلايا الشمسية والطاقة المتجددة، قسم الفيزياء، جامعة شارد، نويدا الكبرى، الهند

الملخص

تم تحضير معقدات الزئبق (II) الجديدة من (2)-(2)-(2-كلوربنزيلدين) هيدرازينيل) بنزوئثيازول) (CHB) مع ليكاندات الفوسفين (dppm، dppe، dppp و dppb)، مما أدى إلى تكوين معقدات تحتوي على الصيغ: $[\text{Hg}_2(\text{CHB})_2(\mu\text{-dppm})_2]\text{Cl}_4$ أو $[\text{Hg}_2(\text{CHB})_2(\mu\text{-phosphine})\text{Cl}_2]\text{Cl}_2$ (حيث تكون الفوسفينات هي dppe و dppp و dppb). حيث ان الشكل الهندسي المقترح حول أيون الفلز هو رباعي السطوح، يسلك ليكاند (CHB) كليكاند ثنائي السن عبر ذرات النتروجين، بينما تسلك الفوسفينات كليكاندات ثنائية السن عبر ذرات P. تم تشخيص

<https://doi.org/10.25130/tjps.v29i2.1568>

المعقدات المحضرة بمختلف التقنيات التحليلية بما في ذلك التوصيلية المولية، أطياف الأشعة تحت الحمراء، أطياف ^1H -، $^{31}\text{P}\{^1\text{H}\}$ -NMR، وأطياف ^{13}C -NMR. بالإضافة إلى ذلك، تم تقييم الفعالية البيولوجية لهذه المعقدات ضد أربعة أنواع من البكتيريا، وهي *Staphylococcus aureus*، *Streptococcus faecalis*، و *Escherichia coli* و *Pseudomonas aeruginosa*. أظهرت بعض المعقدات مستوى تثبيط تراوح بين (5-10 ملم) عند أدنى تركيز مثبت مما يشير على وجود خواص مضادة للبكتيريا محتملة.

Introduction

Benzothiazole is considered one of the prominent heterocyclic compounds derived from benzene. Benzothiazole is characterized by its distinctive chemical structure, as it includes two heteroatoms, nitrogen (N) and sulfur atom (S), located in the pentagonal ring fused to the benzene ring [1]. Benzothiazole compounds and their derivatives have great vital importance in various fields, including the pharmaceutical, agricultural, and environmental industries. Its derivatives are used in various applications based on their unique chemical and biological properties. Thiazole compounds and their derivatives are of great importance due to their wide use in pharmaceutical and agricultural chemistry [2]. 2-Hydrazone benzothiazole is considered an important derivative due to its being considered a nucleus for other organic derivatives as well as for its biological activities. Benzothiazole compounds show electrophilic and nucleophilic properties depending on the resonance structures they possess, as the electrons are distributed throughout the benzothiazole structure, but without the electrons sharing the sulfur atom in some of the resonance structures. Also, the compound 2-benzothiazole hydrazone has been evaluated for its anti-cancer activity in vitro against leukemia, breast cancer and colon cancer [3]. The chemistry and pharmaceutical chemistry of benzothiazole derivatives have aroused great interest due to their diverse bioactivity [4]. Among them are anti-inflammatory, analgesic, and antibacterial properties [5,6].

Recently, benzothiazole analogs linked to hydrazine have been studied in the context of breast cancer and compared with non-cancer cells [7]. Benzothiazole and its derivatives play a pivotal role as components in several important pharmaceutical drugs. They are used in the treatment of various diseases and medical conditions, including fungal infections, systemic disorders, and cancerous tumors. For example, certain derivatives have been employed in the treatment of parasitic diseases such as malaria and amoebiasis [4,5].

Complexes containing benzothiazole ligands are of great importance in various fields. The ligands derived from benzothiazoles are distinguished by their unique structures and their ability to coordinate with various metal elements, which contribute to the properties of these complexes, including stability and size effect, in enhancing the chemical and biological activities of these complexes [8,9]. Also, benzothiazole complexes are of great importance in many chemical and biological applications, as they can be used in catalytic processes, oxidation-

reduction reactions, chemical cleavage reactions, and ring-closing reactions [10,11].

Experimental

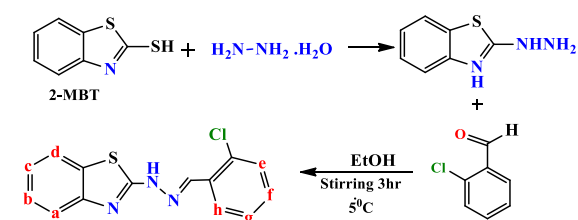
All chemicals and solvents were used as prepared without additional purification in the preparation of ligands and complexes. The melting points of the prepared complexes were determined using an Automatic (SMP30) melting point apparatus. The molar conductivity of freshly prepared complexes in a 10^{-3}M using DMSO as a solvent, it was measured with a digital conductivity meter (Starter 3100c). Elemental analysis for carbon, hydrogen, nitrogen, and sulfur was conducted using an Elementar vario El III CHN elemental analyzer. Infrared (IR) spectra of the complexes were recorded as KBr pellets using a Shimadzu FT-IR8400S spectrophotometer ($400\text{-}4000\text{ cm}^{-1}$). Nuclear magnetic resonance (NMR) spectra were acquired on a Bruker 400 MHz spectrometer, with DMSO-*d*₆ as the solvent.

Preparation of [CHB]

The preparation involved the following steps:

In a round flask, a mixture of 2-mercaptobenzothiazole (2.500 g, 0.0149 mol) and hydrazine (2.500 ml, 0.0149 mol) was combined. The mixture was then heated to $130\text{ }^\circ\text{C}$ and stirred for one and a half hours. During this time, the brown color of the mixture changed, and the distinct smell of H_2S became noticeable. Following this, 4 ml of absolute ethanol was added, and the reaction was allowed to continue for an additional three hours at the same temperature until the mixture became light yellow. After cooling, a white precipitate formed, which was subsequently filtered and washed with cold distilled water and cold absolute ethanol.

To the resulting precipitate, a solution of 2-chlorobenzaldehyde (2.100 g, 0.0149 mol) was introduced. The final mixture was then heated for three hours, resulting in the formation of a light yellow suspension. Finally, the obtained product was oven-dried under reduced pressure. The yield was determined to be 5.34 g (75.21%) [12].



Scheme 1: Ligand preparation equation

(CHB) Yield: (5.34 g, 75.21%). Melting point: $268\text{ }^\circ\text{C}$. FTIR (KBr): 3251 (s), 3064 (m), 1616 (s), 1559 (s), 1542 (m), 1440 (s), 1263 (m), 1132 (m),

<https://doi.org/10.25130/tjps.v29i2.1568>

750 (s), 719 (w), 613, 513. $^1\text{H-NMR}$ (DMSO- d_6) δ (ppm): 12.53(s, 1H, NH), 8.44 (s, 1H, CH), 7.96 (dd, $^3J=1.78$ Hz, 1H, H_a), 7.80 (d, $^3J=7.82$ Hz, 1H, H_c), 7.70 (dd, 1H, H_d) 7.49 (t, $^3J=7.33$ Hz, 2H, H_e, H_f), 7.34 (m, 2H, H_b, H_c), 7.14 (t, $^3J=7.47$ Hz, 1H, H_b),

$^{13}\text{C-NMR}$ (DMSO- d_6) δ (ppm): 167.63, 133.70, 133.43, 131.66, 128.61, 127.24, 126.53, 122.37, 122.08. Molar conductivity ($18.7 \Omega^{-1} \text{cm}^2 \text{mol}^{-1}$).

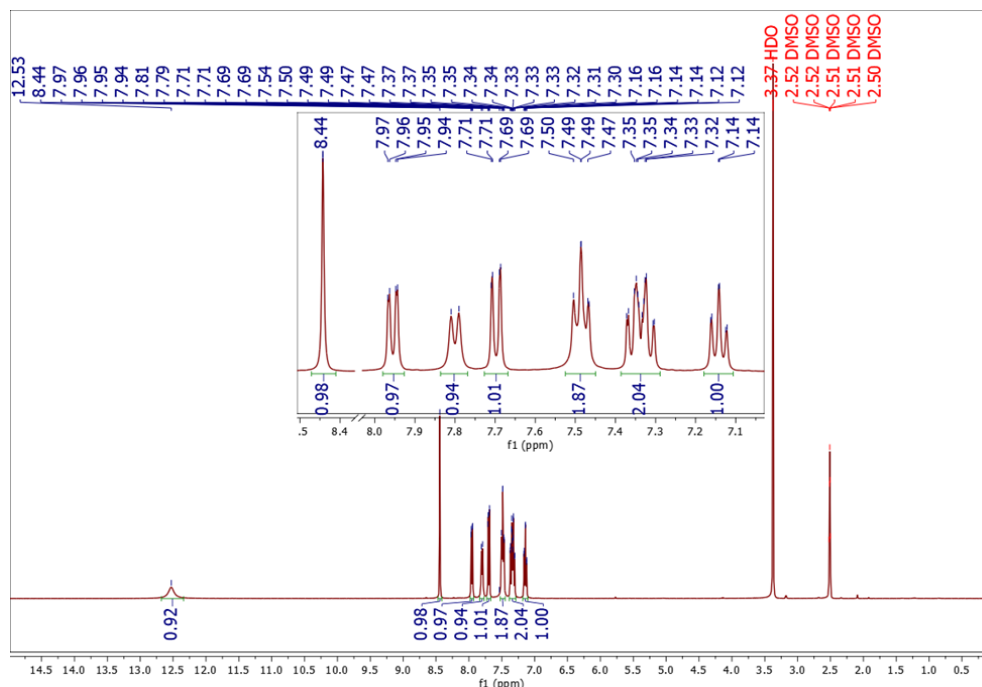


Fig. 1: $^1\text{H-NMR}$ spectrum of the ligand [CHB]

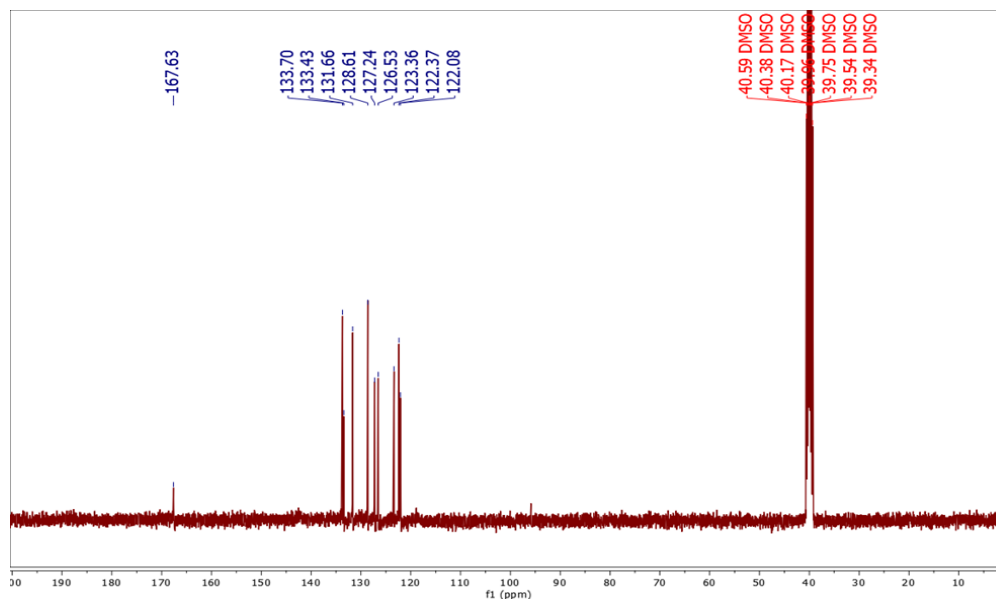


Fig. 2: $^{13}\text{C}\{-^1\text{H}\}$ -NMR spectrum of [CHB]

Synthesis of $[\text{Hg}_2(\text{CHB})_2(\mu\text{-dppm})_2]\text{Cl}_4$

A suspension of (CHB) (0.451 g, 0.0015 mol) in 10 ml of absolute ethanol was added to a solution of mercuric chloride (HgCl_2) (0.424 g, 0.0015 mol) in 15 ml of ethanol. The mixture was stirred for an hour, and then (dppm) (0.576 g, 0.0015 mol) in 15 ml of absolute ethanol was added. The resulting mixture was stirred for two hours, forming a light yellow

suspension. The precipitate was obtained by filtration and subsequently washed with ethanol.

$[\text{Hg}_2(\text{CHB})_2(\mu\text{-dppm})_2]\text{Cl}_4$ (1) White precipitate from ethanol, Yield: (1.33 g, 91.7%). Melting point: 317°C (decomposed). FTIR (KBr): 3249 (m), 3157 (m), 3051 (w), 2952 (w), 1643 (m), 1612 (m), 1566 (s), 1475 (m), 1438 (s), 1263 (m), 1103 (m), 744 (s), 692 (m), 509 (w). $^{31}\text{P}\{^1\text{H}\}$ NMR: $\delta = 22.70$ ppm. $^1\text{H-NMR}$ (DMSO- d_6) δ (ppm): 12.57 (s, 1H, NH), 8.45

<https://doi.org/10.25130/tjps.v29i2.1568>

(S,1H,CH), 7.93 (m, 9H,H_a), 7.80 (d, 1H,H_b), 7.70 (d, ³J=8.00 Hz, 1H,H_d), 7.50 (q, 5H,H_c,H_e), 7.36 (t, 10H,

H_e,H_f), 7.14 (d, ³J=7.56 Hz, 1H,H_b),. Molar conductivity (138.6 Ω⁻¹cm²mol⁻¹).

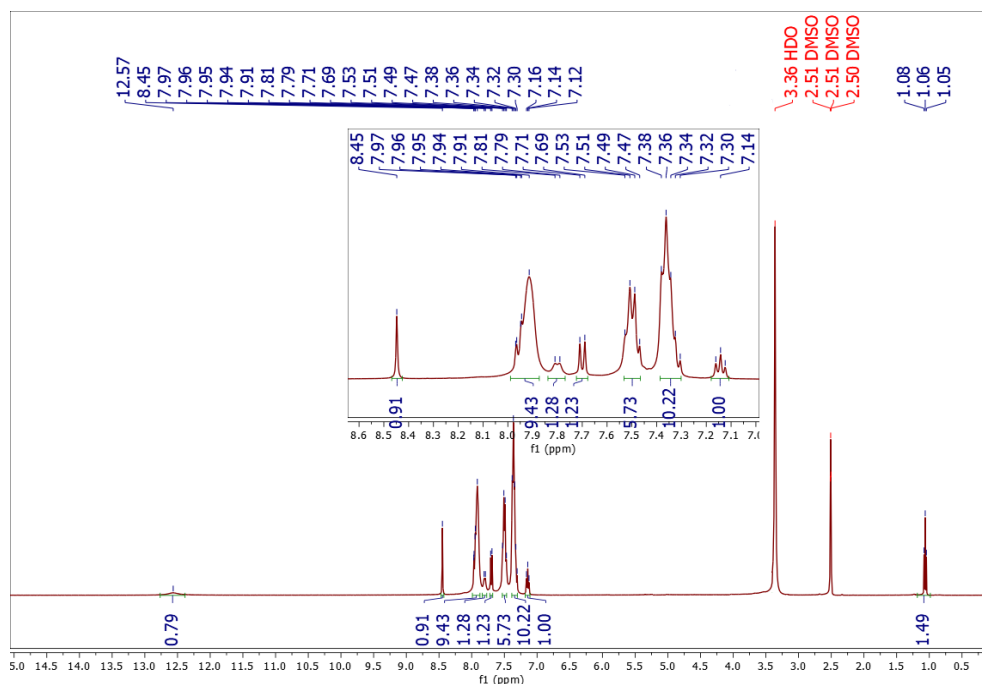


Fig. 3: ¹H-NMR spectrum of [Hg₂(CHB)₂(μ-dppm)₂]Cl₄

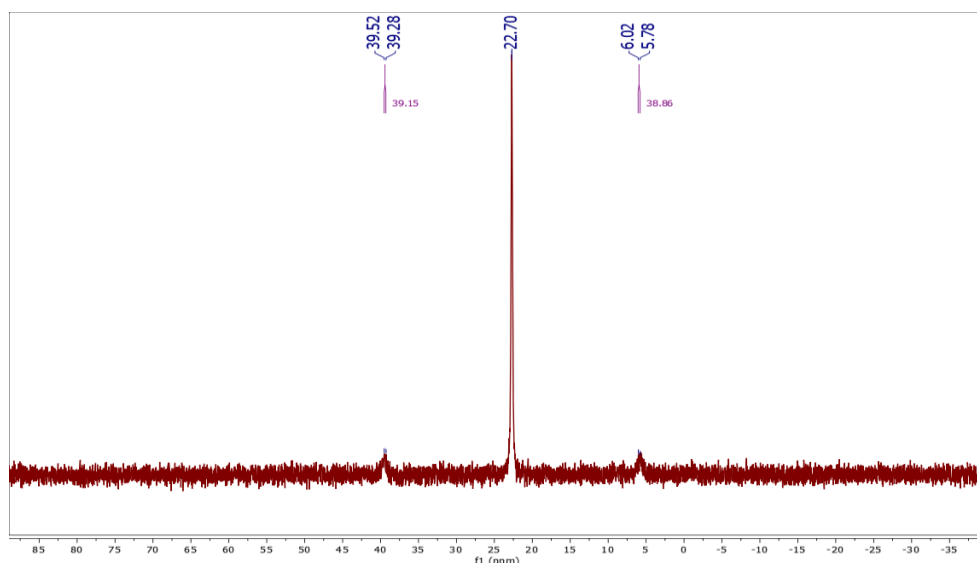


Fig. 4: ³¹P-{¹H}-NMR spectrum of [Hg₂(CHB)₂(μ-dppm)₂]Cl₄

Synthesis of [Hg₂(CHB)₂(μ-dppe)Cl₂]Cl₂ complexes (phos. = dppe, dppp, dppb)

A suspension of (CHB) (0.213 g, 0.770 mmol) in 15 ml of absolute ethanol was added to a solution of mercuric chloride (HgCl₂) (0.209 g, 0.770 mmol) in 10 ml of ethanol, and the mixture was stirred for three hours. Then, a solution of (dppe) (0.147 g, 0.370 mmol) in 15 ml of ethanol was added to it. The final mixture was stirred for two hours, resulting in a pale yellow colored suspension. The crystalline precipitate was filtered, washed with cold ethanol, and dried in an oven under reduced pressure.

[Hg₂(CHB)₂(μ-dppe)Cl₂]Cl₂ (2) Pale yellow precipitate from ethanol, Yield: (0.43 g, 77.1%), Melting point: 326°C (decomposed). FTIR (KBr): 3197 (m), 3139 (m), 3074 (w), 2956 (w), 1625 (s), 1602 (s), 1136 (s), 1400 (w), 1271 (w), 1191 (w), 1103 (s), 750 (s), 725(s), 509(s). ³¹P{¹H} NMR: δ = 37.41 ppm. ¹H-NMR (DMSO-*d*⁶) δ(ppm): 12.56 (s, 1H, NH), 8.44 (s, 1H), 7.95 (d, ³J=7.75 Hz, H_a), 7.79 (t, ³J=7.63 Hz, 5H, H_b), 7.70 (d, 2H, H_d), 7.65 (t, 4H, H_e), 7.49 (t, 2H, H_c), 7.34 (dt, ³J=7.27 Hz, 2H, H_f), 7.14 (t, ³J=7.52 Hz, H_b), (s 3.07, 2CH₂). Molar conductivity (74.2 Ω⁻¹cm²mol⁻¹).

Synthesis of [Hg₂(CHB)₂(μ-dppp)Cl₂]Cl₂ complexes

<https://doi.org/10.25130/tjps.v29i2.1568>

A suspension of (CHB) (0.35 g, 1.2100 mmol) in 10 ml of absolute ethanol was added to a solution of mercuric chloride (HgCl_2) (0.33 g, 1.2100 mmol) in 15 ml of ethanol, and the mixture was stirred for three hours. Then, a solution of (dppp) (0.299 g, 0.0605 mmol) in 20 ml of ethanol was added to it. The final mixture was stirred for two hours, resulting in a white suspension. The crystalline precipitate was filtered, washed with cold ethanol, and dried in an oven under reduced pressure.

[$\text{Hg}_2(\text{CHB})_2(\mu\text{-dppp})\text{Cl}_2\text{Cl}_2$ (3) White precipitate from ethanol, Yield: (0.87 g, 83.1%), Melting point: 317°C (decomposed). FTIR (KBr): 3269 (m), 3139 (m), 3062 (w), 2950 (w), 1647 (s), 1616 (s), 1569 (s), 1440 (s), 1263 (m), 1132 (m), 1018 (w), 750 (s), 719(m), 522(w), 489(w). $^{31}\text{P}\{^1\text{H}\}$ NMR: $\delta = 12.55$ ppm. ^1H -NMR (DMSO- d_6) δ (ppm): 12.59 (s, 1H, NH), 8.46 (s, 1H, CH), 7.95 (dd, $^3J=1.77$ Hz, 1H, H_a), 7.81 (m, 12H, H_b), 7.70 (dd, $^3J=1.18$ Hz, 2H, H_d), 7.48 (m, 2H, H_e, H_c), 7.34 (m, 2H, H_e, H_f), 7.14 (t, 1H, H_b), 2.71 (m, 6H, CH_2 of dppp), 1.75 (d, 3H, CH_2 of dppp). Molar conductivity ($76.7 \Omega^{-1}\text{cm}^2\text{mol}^{-1}$).

[$\text{Hg}_2(\text{CHB})_2(\mu\text{-dppb})\text{Cl}_2\text{Cl}_2$ (4) White precipitate from ethanol, Yield: (0.71 g, 79.4%), Melting point: 319°C. FTIR (KBr): 3226 (s), 3116 (m), 3047 (m), 2856 (w), 1649(s), 1623 (s), 1550 (m), 1475 (s), 1429 (s), 1396 (m), 1110 (w), 742 (s), 688 (s), 582 (w), 445(m). $^{31}\text{P}\{^1\text{H}\}$ NMR: $\delta = 35.30$ ppm. ^1H -NMR (DMSO- d_6) δ (ppm): 12.58 (s, 1H, NH), 8.44 (s, 1H, CH), 7.95 (d, $^3J=7.91$ Hz, 1H, H_a), 7.82 (dd, $^3J=7.48$ Hz, 5H, H_b), 7.69 (d, $^3J=8.21$ Hz, 1H, H_d), 7.62 (dt, 7H, H_g), 7.48 (t, $^3J=7.62$ Hz, 2H, H_c), 7.33 (m, 2H,

H_e, H_f), 7.14 (t, $^3J=7.67$ Hz, 2H, H_b). Molar conductivity ($78.4 \Omega^{-1}\text{cm}^2\text{mol}^{-1}$).

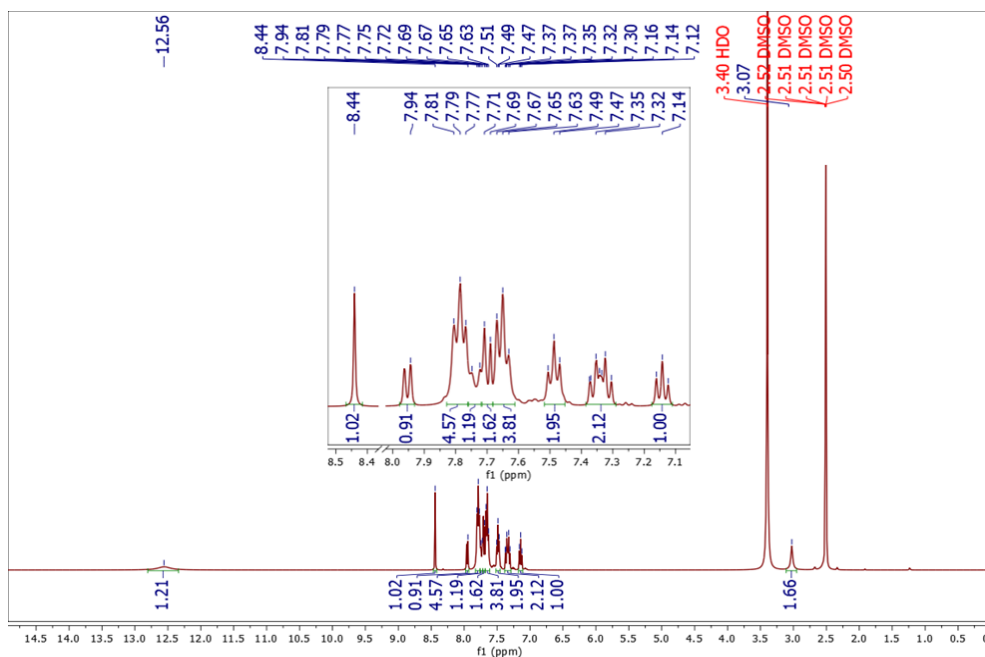
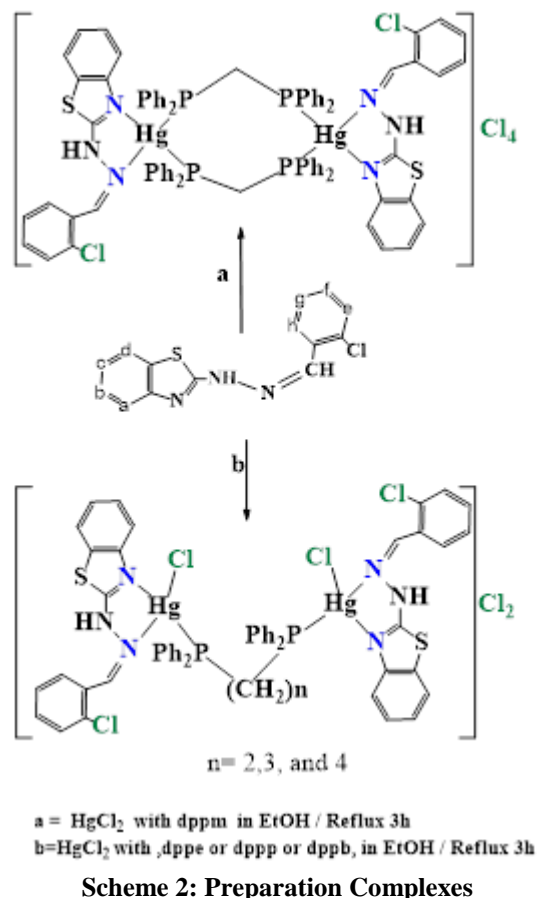


Fig. 5: ^1H -NMR spectrum of $[\text{Hg}_2(\text{CHB})_2(\mu\text{-dppe})\text{Cl}_2]\text{Cl}_2$

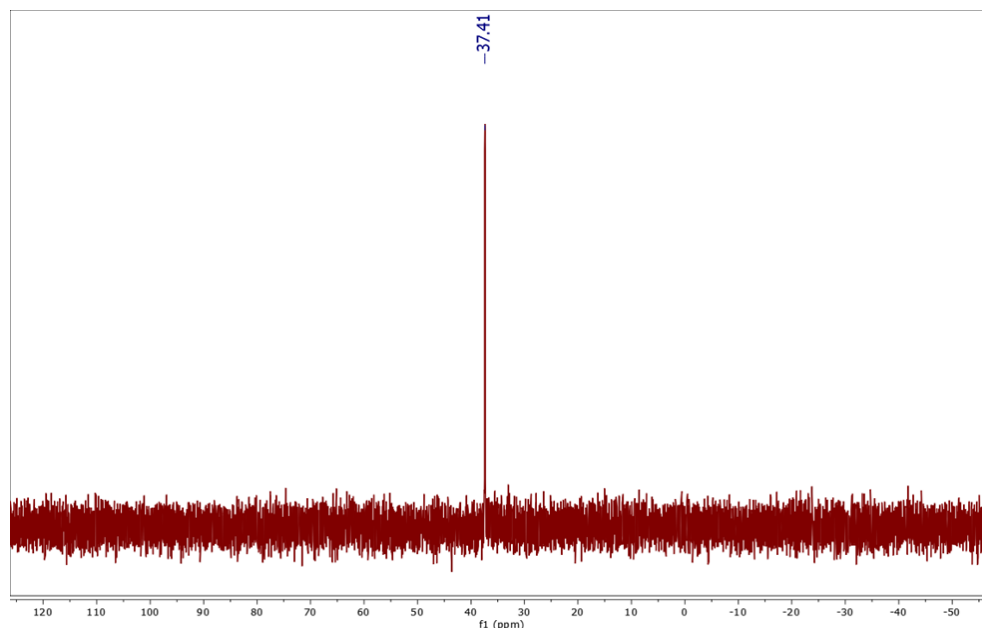


Fig. 6: $^{31}\text{P}\{-^1\text{H}\}$ -NMR spectrum of $[\text{Hg}_2(\text{CHB})_2(\mu\text{-dppe})\text{Cl}_2]\text{Cl}_2$

Results and discussion

The results of the ^{31}P -NMR, ^{13}C -NMR and ^1H -NMR spectra analysis confirmed the validity of the proposed formulas for the studied complexes. The molar conductivity results for complexes (1) indicated that these complexes have non-electrolytic solutions due to their lack of ions outside the coordination sphere, as they exhibited molar conductivities in the range of $18.2 \Omega^{-1}\text{cm}^2\text{mol}^{-1}$ [13]. In the IR spectra, the ligand and prepared complexes showed the NH_2 stretching appeared as two peaks in the range of $3400\text{-}3371 \text{ cm}^{-1}$ and $3315\text{-}3259 \text{ cm}^{-1}$ [14], while the C-N stretching appeared in the range of $1263\text{-}1396 \text{ cm}^{-1}$, the NH stretching appeared in the range of $3251\text{-}3176 \text{ cm}^{-1}$ [15,16]. The C=N stretching group appeared in the range of $1616\text{-}1629 \text{ cm}^{-1}$ [17-18].

Regarding the ^1H -NMR spectrum of ligand (CHB), the proton nuclear magnetic resonance (^1H -NMR) spectrum of the ligand measured in DMSO-*d*₆ as a solvent showed a single signal at a chemical shift ($\delta H=8.44 \text{ ppm}$), attributed to the protons of the CH group, with an integration of one proton. There was also a doublet signal at a chemical shift ($\delta H=7.96 \text{ ppm}$) with a coupling constant of ($^3J_{\text{H-H}}=1.8 \text{ Hz}$), attributed to a proton (H_a), with an integration of one proton. Another doublet signal appeared at ($\delta H=7.80 \text{ ppm}$) with a coupling constant of ($^3J_{\text{H-H}}=7.8 \text{ Hz}$), attributed to a proton (H_b), with an integration of one proton. A doublet signal at ($\delta H=7.70 \text{ ppm}$) with a coupling constant of ($^3J_{\text{H-H}}=7.60 \text{ Hz}$) was attributed to a proton (H_d), with an integration of one proton. A pseudo-triplet signal appeared at ($\delta H=7.34 \text{ ppm}$) and ($\delta H=7.37 \text{ ppm}$) with a coupling constant of ($^3J_{\text{H-H}}=7.53 \text{ Hz}$), attributed to protons (H_c) and (H_f), with an integration of two protons. Additionally, a signal

formed from the fusion of two triplets was observed at ($\delta H=7.28 \text{ ppm}$) and ($\delta H=7.49 \text{ ppm}$) attributed to protons (H_c) and (H_g), with an integration of two protons. Furthermore, a triplet signal appeared at ($\delta H=7.14 \text{ ppm}$) with coupling constants of ($^3J_{\text{H-H}}=1.2 \text{ Hz}$) and ($^3J_{\text{H-H}}=7.6 \text{ Hz}$), attributed to a proton (H_b), with an integration of one proton. The spectrum of the ligand also showed a single signal at ($\delta H=12.53 \text{ ppm}$), attributed to the proton of the NH group, with an integration of one proton.

On the other hand, the ^{13}C -NMR spectrum showed a signal at ($\delta H=167.63 \text{ ppm}$), which was assigned to the carbon atom carrying the C=N group. The signals at ($133.70, 133.43, 131.66, 128.61, 127.24, 126.53, 123.36, 122.37, 122.08 \text{ ppm}$) were attributed to the carbon atoms in the benzene ring.

The ^1H -NMR spectrum of complex (1) measured in dmsO-*d*₆ showed a broad single signal at $\delta H=1.06 \text{ ppm}$, attributed to the protons of the (CH_2) group in (dpmp), with an integration of two protons. Additionally, there was a single signal at $\delta H=8.45 \text{ ppm}$, assigned to the protons of the CH group, with an integration of one proton. The spectrum exhibited a binary signal at $\delta H=7.93 \text{ ppm}$, which overlapped with the phenyl groups in (dpmp), attributed to (H_a) protons, and with an integration of ten protons. Furthermore, a triple signal centered at $\delta H=7.36 \text{ ppm}$, with a coupling constant of 7.62 Hz , was observed, attributed to (H_e)(H_f), and it integrated 10 protons. Two overlapping triads at $\delta H=7.50 \text{ ppm}$, with a coupling constant of 8.04 Hz , were also evident, which were attributed to a proton (H_c) (H_g), and they integrated six protons. Another binary signal at $\delta H=7.70 \text{ ppm}$, with a coupling constant of 8.00 Hz , was identified, assigned to (H_d) protons, and with an integration of one proton. The spectrum displayed a triple signal at $\delta H=7.14 \text{ ppm}$, with a coupling

<https://doi.org/10.25130/tjps.v29i2.1568>

constant of 7.56 Hz, which was attributed to a proton (H_b), and it integrated one proton. Additionally, a binary signal at $\delta H=7.80$ ppm, with a coupling constant of 7.85 Hz, was observed, assigned to a proton (H_h), and it integrated one proton. Finally, the spectrum showed a single signal at $\delta H=12.57$ ppm, attributed to the (NH) group, with an integration of one proton. Furthermore, the ^{31}P -NMR spectrum displayed a singlet signal at a positive value of $\delta H=22.70$ ppm, attributed to the phosphorus atom in the coordinated (dppm) ligand, which is associated with the central metal ion [18].

The 1H -NMR spectrum of complexes (2, 3, 4) indicated a ratio of integration suggesting a dinuclear structure, where there are two moles of the ligand (CHB) to one mole of phosphine.

For complex (2), the 1H -NMR spectrum measured in $DMSO-d^6$ showed a broad single signal at $\delta H=3.07$ ppm, attributed to the protons of the (CH_2) group in (dppe) with an integration of two protons. Additionally, there was a single signal at $\delta H=8.44$ ppm, assigned to the protons of the CH group, with an integration of one proton. The spectrum displayed a binary signal at $\delta H=7.95$ ppm, with a coupling constant of 7.75 Hz, attributed to (H_a) protons and with an integration of one proton. Another binary signal centered at $\delta H=7.34$ ppm appeared, with a coupling constant of 7.27 Hz, which overlapped with phosphine and was attributed to (H_c) with an integration of two protons. A triple signal at $\delta H=7.65$ ppm, with a coupling constant of 7.64 Hz, was also evident, attributed to a proton (H_c) (H_g) and it integrated four protons. Furthermore, a binary signal at $\delta H=7.49$ ppm, with a coupling constant of 7.41 Hz, was identified, assigned to protons (H_f), and it integrated one proton. The spectrum showed a binary signal at $\delta H=7.70$ ppm, with a coupling constant of 8.00 Hz, attributed to (H_d) protons and with an integration of one proton. A triple signal at $\delta H=7.14$ ppm, with a coupling constant of 7.52 Hz, was observed, which was attributed to a proton (H_b) and with an integration of one proton. The spectrum exhibited a duality at $\delta H=7.79$ ppm, with a coupling constant of 7.63 Hz, representing a proton (H_h) and with an integration of five protons. Lastly, the spectrum showed a single signal at $\delta H=12.56$ ppm, attributed to the (NH) group, with an integration of one proton.

Moreover, the ^{31}P -NMR spectrum showed a singlet signal at a positive value of $\delta P=37.41$ ppm, indicating that the phosphorus atoms in dppe are equivalent and bridged with the Hg ion in the dinuclear complex [19]. The complex (3) exhibited a broad single signal at $\delta H=1.86$ ppm, which was attributed to the two protons of the (CH_2) intermediate group in (dppp) with an integration of two protons. Additionally, it showed a broad single signal at $\delta H=3.07$ ppm, attributed to the protons of the (CH_2) terminal group in (dppp) with an integration of four protons. The

spectrum displayed a single signal at $\delta H=8.44$ ppm, which was assigned to the protons of the CH group in ligand with an integration of one proton. Moreover, there was a doublet signal at $\delta H=7.95$ ppm with a coupling constant of 7.85 Hz, attributed to (H_a) protons and it integrated one proton. A binary signal centered at $\delta H=7.80$ ppm appeared with a coupling constant of 8.11 Hz, attributed to a proton (H_h) and with an integration of five aromatic protons. The spectrum also showed a binary signal interfering with phosphine at $\delta H=7.70$ ppm, with a coupling constant of 8.6 Hz, which was attributed to a proton (H_d) and it integrated one proton. Additionally, there was a triple signal at $\delta H=7.55$ ppm with a coupling constant of 7.52 Hz, attributed to a proton (H_c) and it integrated four protons. Another triple signal at $\delta H=7.14$ ppm with a coupling constant of 7.52 Hz appeared, which was attributed to a proton (H_b) and it integrated one proton. The spectrum exhibited a triple overlapping signal with phosphine at $\delta H=7.34$ ppm, with a coupling constant of 7.92 Hz, attributed to a proton (H_f) and it integrated two protons. Moreover, a binary signal at $\delta H=7.63$ ppm was attributed to a proton (H_e) and it integrated two protons. A triple signal at $\delta H=7.49$ ppm was attributed to a proton (H_g) and it integrated two protons. Finally, the spectrum showed a single signal at $\delta H=12.53$ ppm, attributed to the (NH) group, and with an integration of one proton. Moreover, the ^{31}P -NMR spectrum showed a singlet signal at a positive value of $\delta P=31.17$ ppm, indicating that the phosphorus atoms in dppp are equivalent and bridged with the Hg ion in the dinuclear complex [18]. In complex (4), a broad single signal at $\delta H=1.68$ ppm, which was attributed to the four protons of the ($2CH_2$) intermediate group in (dppb). Additionally, it showed a broad single signal at $\delta H=2.89$ ppm, attributed to the protons of the ($2CH_2$) terminal group in (dppb) with an integration of four protons. The spectrum displayed a single signal at $\delta H=8.44$ ppm, which was assigned to the protons of the CH group with an integration of one proton. Moreover, there was a doublet signal at $\delta H=7.95$ ppm with a coupling constant of 7.91 Hz, attributed to (H_a) protons and it integrated one proton. A signal centered at $\delta H=7.82$ ppm attributed to a protons ($Ph+H_h$) and with an integration of five protons. The spectrum also showed a doublet signal interfering with phosphine at $\delta H=7.69$ ppm, with a coupling constant of 8.21 Hz, which was attributed to a proton (H_d) and it integrated one proton. Additionally, a multiplet centered at $\delta H=7.62$ ppm with integrated 7 protons was attributed to (Ph) protons of dppb, there was a triple signal at $\delta H=7.48$ ppm with a coupling constant of 7.62 Hz, attributed to a proton (H_f+H_g) and it integrated two protons. Another multiplet signal centered at $\delta H=7.33$ ppm which was attributed to a proton (H_c+H_h) and it integrated two protons. The spectrum exhibited a triple signal at $\delta H=7.14$ ppm, with a coupling constant of 7.67 Hz, attributed to a

<https://doi.org/10.25130/tjps.v29i2.1568>

proton (H_b) and it integrated two protons. Finally, the spectrum showed a single signal at $\delta H=12.53$ ppm, attributed to the (NH) group, and with an integration of one proton.

Additionally, the ^{31}P -NMR spectrum showed a singlet signal at a positive value of $\delta P=35.30$ ppm, indicating that the phosphorus atoms in dppb are equivalent and bridged with the Hg ion in the dinuclear complex[20].

SEM Study

This technique was employed to investigate the structure, surface characteristics, particle shape and size. The electron microscope captured images of the surfaces of metal complexes, revealing distinct differences in crystal structures and surface homogeneity. In SEM analysis, reliance was placed on surface image distance and magnification power.

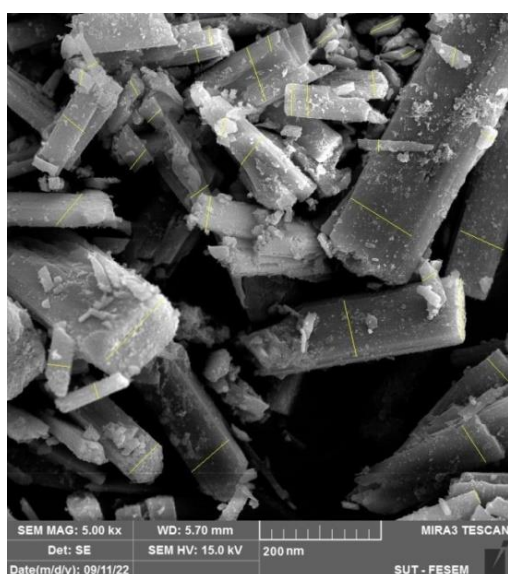
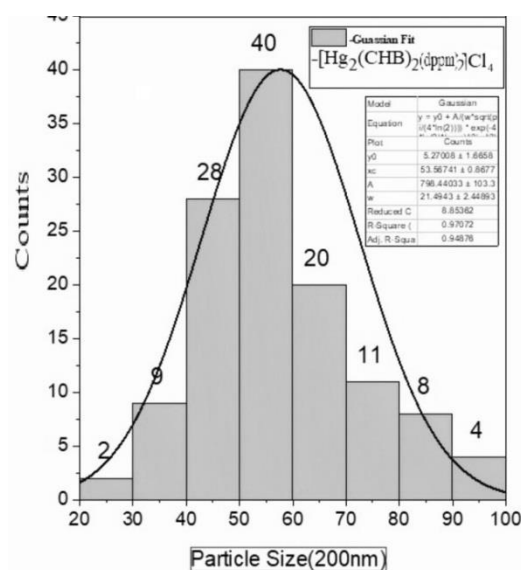


Fig. 7: SEM image of the complex $[Hg_2(CHB)_2\mu-(dppm)_2]Cl_4$ at 200nm, and the particle sizes and Gaussian Fit curve for the complex $[Hg_2(CHB)_2\mu-(dppm)_2]Cl_4$ at 200nm



The SEM analysis of the complex $[Hg_2(CHB)_2\mu-(dppe)Cl_2]Cl_2$, as illustrated in Figure (8), utilized a surface image area of (500 nm) and a magnification power of (MAG: 70.0KX). The radii were

represented in the Gaussian Fit curve, revealing peak radii of the complex particles at (87.49 nm), placing them among the nanocrystals.

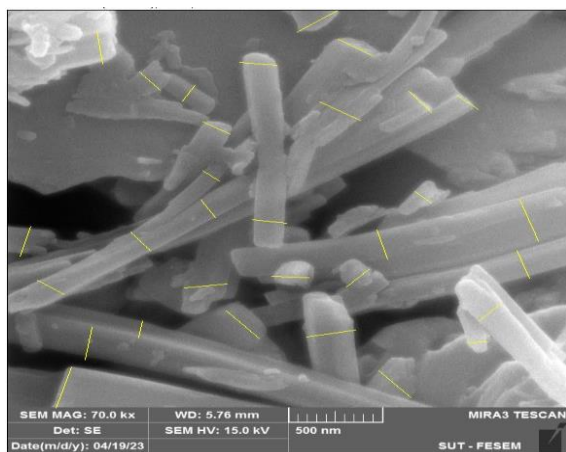
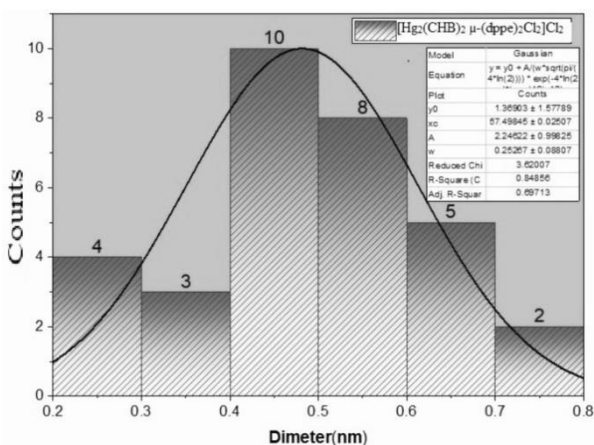


Fig. 8: SEM image of the complex $[Hg_2(CHB)_2\mu-(dppe)Cl_2]Cl_2$ at 500nm, and the particle sizes and Gaussian Fit curve for the complex $[Hg_2(CHB)_2\mu-(dppe)Cl_2]Cl_2$ at 500nm



<https://doi.org/10.25130/tjps.v29i2.1568>

The SEM analysis of the complex $[\text{Hg}_2(\text{CHB})_2(\mu\text{-dppp})\text{Cl}_2]$, depicted in Figure (9), employed a surface image area of (10 μm) and a magnification power of (MAG: 5.00Kx) to visualize the radii displayed in the

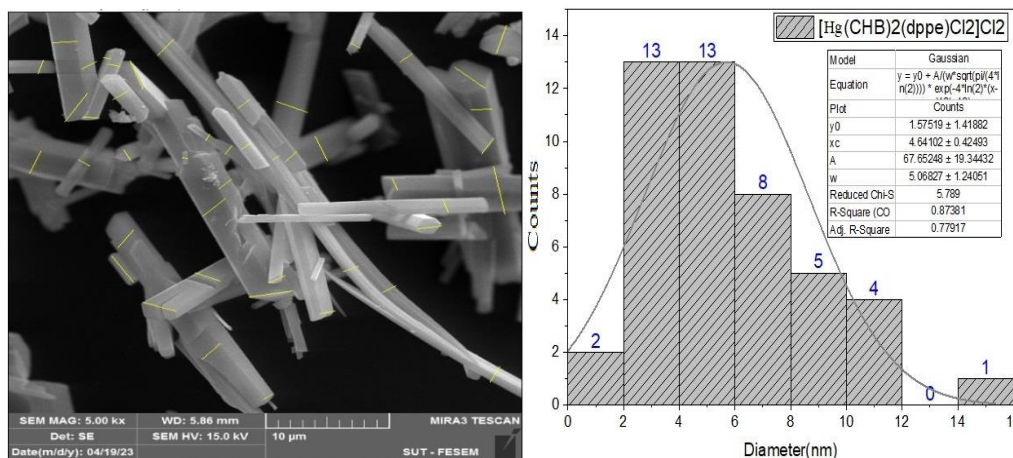


Fig. 9: SEM image of the complex $[\text{Hg}_2(\text{CHB})_2(\mu\text{-dppp})\text{Cl}_2]\text{Cl}_2$ at 10 μm , and the particle sizes and Gaussian Fit curve for the complex $[\text{Hg}_2(\text{CHB})_2(\mu\text{-dppp})\text{Cl}_2]\text{Cl}_2$ at 10 μm

The SEM analysis of the complex $[\text{Hg}_2(\text{CHB})_2(\mu\text{-dppb})\text{Cl}_2]\text{Cl}_2$, as illustrated in Figure (10), utilized a surface image area of (1 μm) and a magnification power of (HV: 15.0KV). The radii were displayed in

Gaussian curve. The calculated radii for the complex particles were (464 nm), placing them within the nanocrystal range.

the Gaussian curve (Gaussian Fit). The peak radii of the complex particles were (426 nm), placing them among the nanowires.

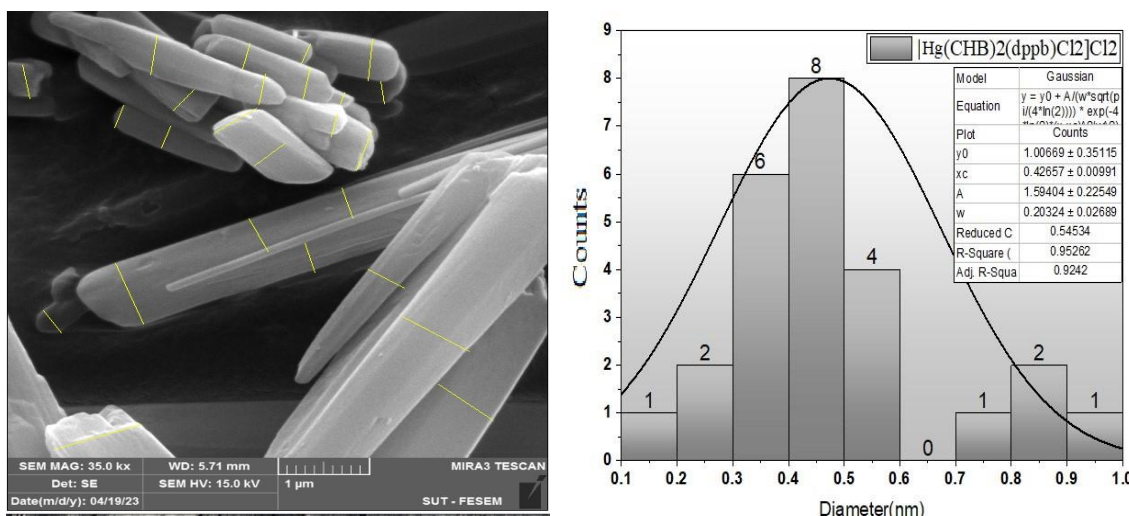


Fig. 10: SEM image of the complex $[\text{Hg}_2(\text{CHB})_2(\mu\text{-dppb})\text{Cl}_2]\text{Cl}_2$ at 1 μm , and the particle sizes and Gaussian Fit curve for the complex $[\text{Hg}_2(\text{CHB})_2(\mu\text{-dppb})\text{Cl}_2]\text{Cl}_2$ at 1 μm

Spectroscopy Energy-dispersive X-ray(EDX)

The EDX technique is an excellent method for elemental analysis, as it detects X-rays emitted by each element upon exposure to accelerated electrons. This technique can also serve as a reliable quantitative analysis tool, especially for atoms and atomic weights. Its calculations are particularly accurate, primarily measuring the surface of the outer layer only [22].

EDX dispersion spectroscopy analysis provided a qualitative analysis of the complex $[\text{Hg}(\text{CHB})_2\text{Cl}_2]$ using an SEM image of size (25 μm) with a magnification power of (MAG: 350KX), as depicted

in Figure (11,a). The presence of peaks in the analysis indicates the existence of CN, Cl, and Hg.

Qualitative analysis of the EDX correlation spectroscopy for the $[\text{Hg}_2(\text{CHB})_2(\text{dppm})\text{Cl}_4]$ complex revealed an SEM image with a size of (5 μm) and a magnification power of (MAG: 350KX), as illustrated in Figure (11,b).

EDX dispersion spectroscopy analysis similarly presented a qualitative analysis of the $[\text{Hg}_2(\text{CHB})_2(\mu\text{-dppe})\text{Cl}_2]\text{Cl}_2$ complex using an SEM image with a size of (25 μm) and a magnification power of (MAG: 350KX), as depicted in Figure (11,c).

The EDX dispersion spectroscopy analysis demonstrated a qualitative analysis of the complex

<https://doi.org/10.25130/tjps.v29i2.1568>

[Hg₂(CHB)₂μ-(dppp)Cl₂]Cl₂ using an SEM image with a size of (25 μm) and a magnification power of

(MAG: 350KX), as depicted in Figure (11,d).

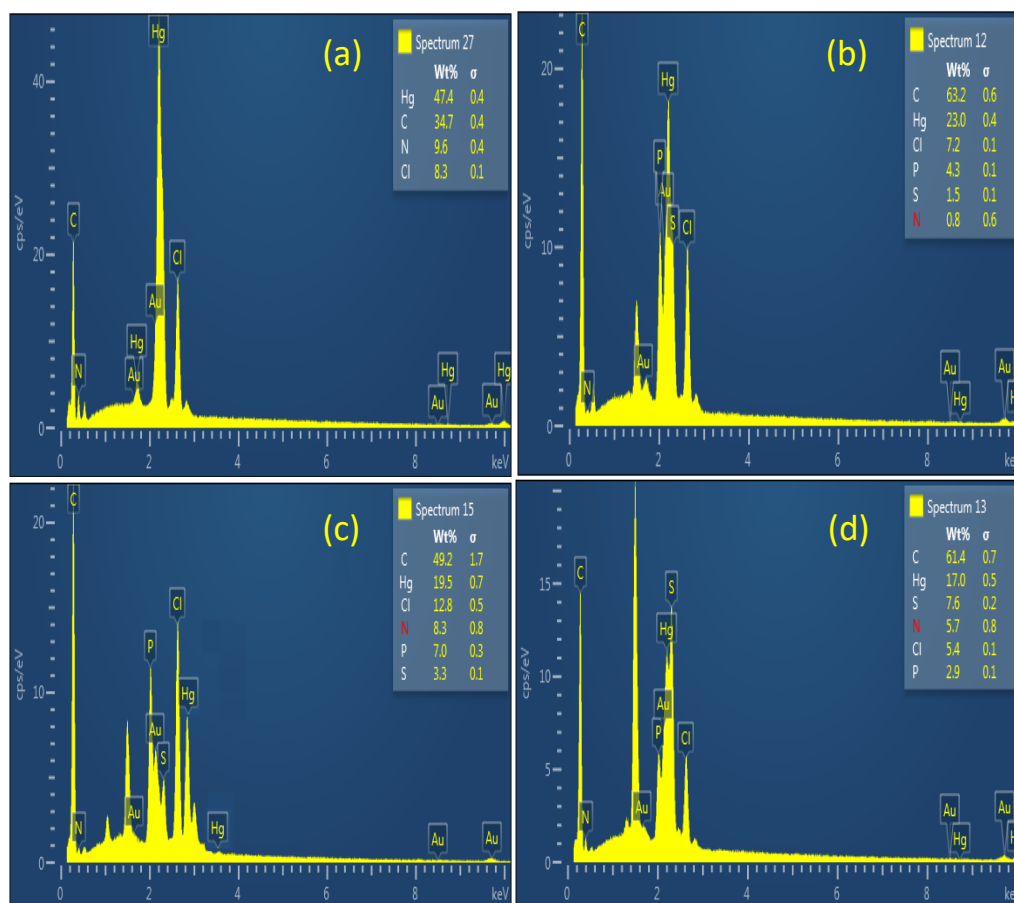


Fig. 11: Elemental structure of the complexes: (a) [Hg(CHB)₂Cl₂], (b) [Hg₂(CHB)₂μ-(dppm)₂]Cl₄, (c) [Hg₂(CHB)₂μ-(dppe)Cl₂]Cl₂, (d) [Hg₂(CHB)₂μ-(dppp)Cl₂]Cl₂

Spectroscopy diffraction X-ray(XRD)

The X-ray diffraction results for the powder of some studied complexes revealed a degree of crystallinity ranging between (47.750% to 56.409%). This calculation was based on the ratios of the total areas under the crystalline peaks (Ac) divided by the total area (Ac + Aa), where (Aa) represents the area under

the baseline. These calculations were performed using the Orgenlab program. The obtained results align with the surface images of the complexes obtained through SEM technology, as illustrated in Table (1), which provides insights into the crystallization of the studied complexes[23].

Table 1: Degree of crystallinity for some prepared complexes

Complexes	Total area under the crystal (Ac) peaks	Total total area (Ac+Aa)	(%) Degree of crystallinity [Ac/Ac+Aa]
[Hg ₂ (CHB) ₂ (μ-dppm) ₂]Cl ₄	11273.01	23101.330	48.798
[Hg ₂ (CHB) ₂ (μ-dppp)Cl ₂]Cl ₂	7845.985	16431.275	47.750
[Hg ₂ (CHB) ₂ (μ-dppe)Cl ₂]Cl ₂	8067.852	14302.367	56.409
[Pd ₂ (CHB) ₂ (μ-dppb)Cl ₂]Cl ₂	6621.795	12717.115	52.069

The results for the studied complexes revealed an average crystal size ranging from (52.315 to 15.367 nm). This corroborates the SEM results, indicating that these complexes consist of nanoparticles within their crystalline structures, even if they are in the

form of aggregates, particles, wires, or nanocrystals, as depicted in the Figures (12). The table provides information on the reflection angles and half-widths of the reflection band for the prepared complexes.

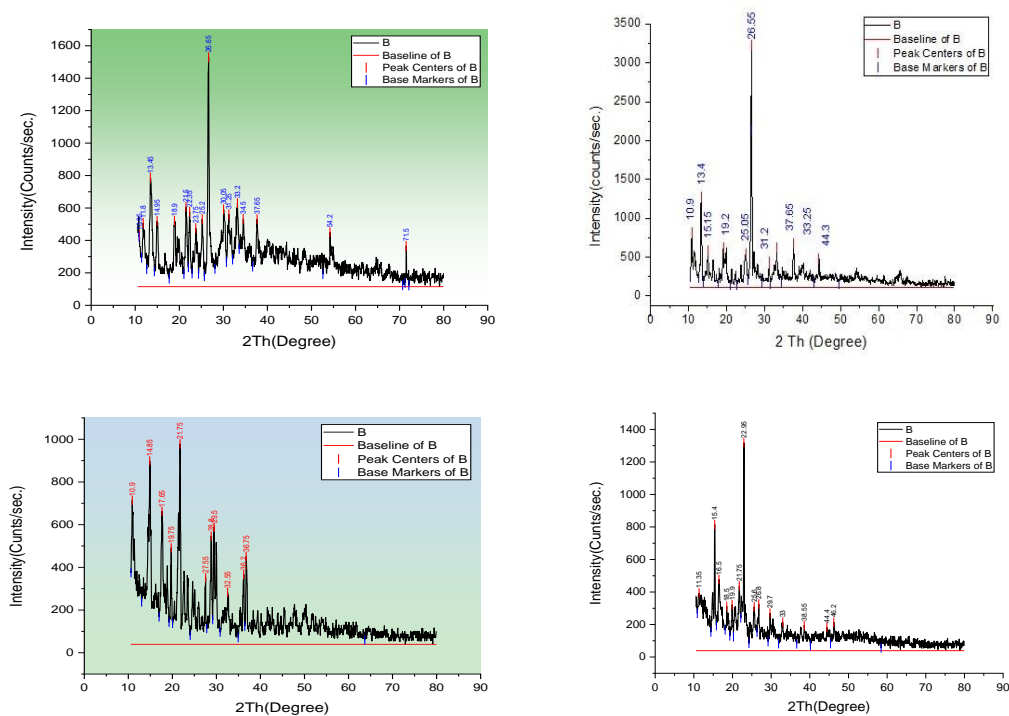


Fig. 12: X-ray diffraction diagram for the complexes

Biological activity

Although mercury compounds are toxic, studies are continuing to prepare new complexes that have biological antibacterial activity [23-25], which encouraged studying the effectiveness of the complexes prepared in this research. Solutions of previously prepared copper and mercury complexes, using DMSO as a solvent, were tested at three concentrations (10^{-4} , 10^{-3} , 10^{-2} g/mol) for their biological activity employing the Agar-well diffusion method. The chosen bacterial species included two types of gram-negative bacteria and two types of gram-positive bacteria, all pathogenic to humans and animals [26,27].

The results, presented in Table (2), indicated that all solutions exhibited antimicrobial activity against the selected bacterial species, even in cases where some bacteria were resistant to antibiotics. The microbial

inhibition zones of the solutions varied from 5 mm to 25 mm, signifying different levels of biological effectiveness depending on the concentrations of the solutions.

At the lowest concentration (10^{-4} g/mol), the complexes demonstrated ineffectiveness against the selected bacterial species. However, the complex $[\text{Hg}_2(\text{CHB})_2\mu\text{-}(\text{dppm})_2]\text{Cl}_4$ exhibited the highest inhibition rate of (25 mm) at a concentration of 10^{-2} g/mol, while the complex $[\text{Hg}(\text{CHB})_2\text{Cl}_2]$ displayed the highest inhibition rate (17 mm) for Gram-negative bacteria at the lowest concentration.

For gram-positive bacteria, the complex $[\text{Hg}_2(\text{CHB})_2\mu\text{-}(\text{dppp})\text{Cl}_2]\text{Cl}_2$ showed the highest inhibition rate (20 mm) at a concentration of 10^{-3} g/mol, whereas the two complexes $[\text{Hg}_2(\text{CHB})_2\mu\text{-}(\text{dppb})\text{Cl}_2]\text{Cl}_2$ exhibited an inhibition rate of 10 mm at the lowest concentration.

Table 2: Biogeological activity for some prepared complexes

Complexes	Conc.	<i>Pseudomonas aeruginosa</i> (-)	<i>Escherichia coli</i> (-)	<i>Staphylococcus aureus</i> (+)	<i>Streptococcus faecalis</i> (+)
[CHB]	10 ⁻²	15	23	10	14
	10 ⁻³	10	12	5	10
	10 ⁻⁴	6	8	NIZ	6
[Hg(CHB) ₂ Cl ₂]	10 ⁻²	25	9	17	10
	10 ⁻³	9	5	7	5
	10 ⁻⁴	5	NIZ	4	NIZ
[Hg ₂ (CHB) ₂ μ-(dppm) ₂ Cl ₄]	10 ⁻²	25	17	18	16
	10 ⁻³	10	8	10	6
	10 ⁻⁴	5	NIZ	6	NIZ
[Hg ₂ (CHB) ₂ μ-(dppe)Cl ₂ Cl ₂]	10 ⁻²	16	12	10	14
	10 ⁻³	10	7	5	8
	10 ⁻⁴	6	NIZ	NIZ	5
[Hg ₂ (CHB) ₂ μ-(dppp)Cl ₂ Cl ₂]	10 ⁻²	20	13	25	16
	10 ⁻³	10	20	15	10
	10 ⁻⁴	7	5	10	5
[Hg ₂ (CHB) ₂ μ-(dppb)Cl ₂ Cl ₂]	10 ⁻²	20	20	20	20
	10 ⁻³	10	14	15	15
	10 ⁻⁴	8	10	10	10

NIZ: No Inhibition Zone

Conclusions

This study revealed that the prepared ligand (CHB) exhibits a bidentate behavior in all synthesized complexes through the nitrogen of the benzothiazole ring and the nitrogen of the azomethine group. Meanwhile, phosphines exhibit a bridging bidentate behavior in the binuclear complexes, with a

tetrahedral geometry around the mercury ion. Surface studies of the prepared complexes indicated nanocrystalline structures with good crystallinity. Furthermore, antibacterial activity studies demonstrated significant effectiveness for the prepared complexes, particularly at lower inhibitory concentrations.

References

- [1] Titvinidze, G., Jishkariani, D., Andronikashvili, E., & Takaishvili, N. (2021). Synthesis, Structural Characterization, and Spectroscopic Properties of Benzimidazole Derivatives. *Molecules*, 26(3), 855.
- [2] Kamat, V., Kotian, A., Nevrekar, A., Naik, K., Kokare, D., & Revankar, V. K. In situ oxidation triggered heteroleptically deprotonated cobalt(III) and homoleptic Nickel(II) complexes of diacetyl monoxime derived tri-nitrogen chelators; Synthesis, molecular structures and biological assay. *Inorganica Chimica Acta*, (2017), 466: 625-631.
- [3] Moharir, S. P., Undegaonkar, M. G., Sinkar, S. N., & Mirgane, S. R. Green and Efficient Synthesis, Characterization and Antimicrobial Activity of Transition Metal complexes of Novel Schiff base ligand derived from 2-hydrazino Benzothiazole and Benzil. *Journal of Chemistry and Chemical Science*, 43-51, (2021).
- [4] Kaur R, Rani S, Mahajan P, et al. Benzimidazole: A Medicinal Marvel. *European Journal of Medicinal Chemistry*. 2020; 185: 111791.
- [5] Rathore S, Verma AK, Goel N, et al. Benzimidazole: A Promising Scaffold for Drug Development. *European Journal of Medicinal Chemistry*. 2019; 174: 443-456.
- [6] Reddy PR, Reddy GS, Reddy CS, et al. Benzimidazole and Its Derivatives as Promising Agrochemicals: An Overview. *Journal of Chemical Sciences*. 2018; 130(5): 1-13.
- [7] Kumar S, Sharma N, Singh D. Benzimidazole: An Insight into Its Versatile Biological Applications. *Journal of Saudi Chemical Society*. 2018; 22(7): 787-805.
- [8] Zhuo S, He Q, Luo X. Benzimidazole-based Metal-Organic Frameworks: Design, Synthesis, and Applications. *Coordination Chemistry Reviews*. 2021; 446: 214175.
- [9] Ahmad S, Raza ZA, McKee V, et al. Benzimidazole-based Metal-Organic Frameworks: Synthesis, Characterization, and Applications in Gas Storage and Separation. *Journal of Materials Chemistry A*. 2020; 8(27): 13280-13309.
- [10] Ferraz RS, Pereira MM, Oliveira SLC, et al. Benzimidazole and its Derivatives as Versatile Scaffolds for Catalysis. *ACS Catalysis*. 2022; 12(5): 4591-4616.
- [11] Xu B, Dong Y, Fu L, et al. Benzimidazole Derivatives as Catalysts for Organic Transformations. *Catalysts*. 2018; 8(6): 233.
- [12] Mohammed, A. A., Mohammed, H. H., Mustafa, T., & Mageed, Z. N. (2022). Synthesis and biological activity of 2-(4, 5-dihydro-1H-pyrazol-1-yl)-1, 3-

<https://doi.org/10.25130/tjps.v29i2.1568>

benzothiazole derivatives. *Journal of Kufa for Chemical Sciences*, 2(8), 109-126.

[13] ALI, Imran; WANI, Waseem A.; SALEEM, Kishwar. Empirical formulae to molecular structures of metal complexes by molar conductance. *Synthesis and reactivity in inorganic, metal-organic, and nano-metal chemistry*, 2013, 43.9: 1162-1170.

[14] Hassan JA, Rasheed MK. Synthesis and characterization of some benzimidazole derivatives from 4-methyl ortho-phenylene diamine and evaluating their effectiveness against bacteria and fungi. In AIP Conference Proceedings 2022 Nov 8 (Vol. 2394, No. 1). AIP Publishing.

[15] Marinescu M, Cintează LO, Marton GI, Chifiriuc MC, Popa M, Stănculescu I, Zălaru CM, Stavarache CE. Synthesis, density functional theory study and in vitro antimicrobial evaluation of new benzimidazole Mannich bases. *BMC chemistry*. 2020 Dec;14(1):1-6.

[16] Razaghi Kashani O, Amiri S, Hosseini-zori M. Self-Healing and Anti-Corrosion Nanocomposite Coatings Based on Polyurethane Nanocapsules containing Mercapto Benzimidazole. *Journal of Nanostructures*. 2022 Jul 1;12(3):726-37.

[17] Salih MM, Irzoqi AA, Alasadi YK, Mensoor MK. Synthesis, Characterization and Antibacterial Activity of some Hg (II) Complexes with Mixed Benzyl 2-(2-oxoindolin-3-ylidene) Hydrazinecarbodithioate and Phosphines or Amines Ligands: doi. org/10.26538/tjnpr/v5i5. 17. *Tropical Journal of Natural Product Research (TJNPR)*. 2021 May 1;5(5):895-901.

[18] Irzoqi AA, Salman FA, Alasadi YK, Alheety MA. Synthesis and Structural Characterization of Palladium (II) Mixed-Ligand Complexes of N-(Benzothiazol-2-yl) benzamide and 1, 2-Bis (diphenylphosphino) ethane. *Inorganic Chemistry*. 2021 Dec 9;60(24):18854-8.

[19] Irzoqi AA, Salih MM, Jirjes HM, Mensoor MK. Synthesis, Characterization, and Antibacterial Activity of Complexes of Hg (II) with Mixtures of 3-Hydranoindolin-2-one and Diphosphine, or Diimine Ligands. *Russian Journal of General Chemistry*. 2020 Jun;90:1069-73.

[20] Jirjes, H. M., Irzoqi, A. A., Al-Doori, L. A., Alheety, M. A., & Singh, P. K. Nano Cadmium(II)-

benzyl benzothiazol-2-ylcarbamodithioate complexes: Synthesis, characterization, anti-cancer and antibacterial studies. *Inorganic Chemistry Communications*, (2022), 135: 109110.

[21] Reimer, Ludwig. "Scanning electron microscopy: physics of image formation and microanalysis." *Measurement Science and Technology* 11, no. 12 (2000): 1826-1826.

[22] Polifke, Wolfgang; Paschereit, Christian Oliver; Döbbeling, Klaus. Constructive and destructive interference of acoustic and entropy waves in a premixed combustor with a choked exit. *Int. J. Acoust. Vib.*, (2001), 6.3: 135-146.

[23] Abdolhi N, Aghaei M, Soltani A, Mighani H, Ghaemi EA, Javan MB, Khalaji AD, Sharbati S, Shafipour M, Balakheyli H. Synthesis and antibacterial activities of novel Hg (II) and Zn (II) complexes of bis (thiosemicarbazone) acenaphthenequinone loaded to MWCNTs. *Journal of Structural Chemistry*. 2019 May;60:845-53.

[24] Ltaief H, Mahroug A, Azaza YB, Nasri M, Graça MP, Belhouchet M. New binuclear mercury complex: Synthesis, supramolecular structure, physico-chemical characterizations and antibacterial activity. *Journal of Molecular Structure*. 2022 Feb 15;1250:131829.

[25] Alshater H, Al-Sulami AI, Aly SA, Abdalla EM, Sakr MA, Hassan SS. Antitumor and Antibacterial Activity of Ni (II), Cu (II), Ag (I), and Hg (II) Complexes with Ligand Derived from Thiosemicarbazones: Characterization and Theoretical Studies. *Molecules*. 2023 Mar 13;28(6):2590.

[26] Muder, R. R., Brennen, C., Rihs, J. D., Wagener, M. M., Obman, A., Obman, A., ... & Yu, V. L. Isolation of *Staphylococcus aureus* from the urinary tract: association of isolation with symptomatic urinary tract infection and subsequent staphylococcal bacteremia. *Clinical infectious diseases*, (2006), 42.1: 46-50.

[27] Rôças, Isabela N.; Siqueira JR, José F.; Santos, Kátia RN. Association of *Enterococcus faecalis* with different forms of periradicular diseases. *Journal of endodontics*, (2004), 30.5: 315-320.